THE JOURNAL OF BIOLOGICAL CHEMISTRY VOL. 288, NO. 22, pp. 15581–15589, May 31, 2013

Facilitated Hyperpolarization Signaling in Vascular Smooth Muscle-overexpressing TRIC-A Channels*[S]

Received for publication, November 11, 2012, and in revised form, March 24, 2013 Published, JBC Papers in Press, April 16, 2013, DOI 10.1074/jbc.M112.435396

Shengchen Tao[‡1], Daiju Yamazaki[‡§1], Shinji Komazaki[¶], Chengzhu Zhao[‡], Tsunaki Iida[‡], Sho Kakizawa[‡], Yuji Imaizumi[‖], and Hiroshi Takeshima[‡§2]

From the [‡]Graduate School of Pharmaceutical Sciences and [§]Center for the Promotion of Interdisciplinary Education and Research, Kyoto University, Kyoto 606-8501, Japan, [¶]Saitama Medical University, Saitama 350-0495, Japan , and the [‖]Graduate School of Pharmaceutical Sciences, Nagoya City University, Aichi 467-8603, Japan

Background: TRIC channels likely mediate counter-K^+ movements during store Ca^{2+} release, but their roles are unknown in many cell types.
Results: Smooth muscle-specific *Tric-a*-transgenic mice developed hypotension due to facilitated hyperpolarization signaling in vascular muscle.
Conclusion: TRIC-A channels facilitate Ca^{2+} spark generation in vascular muscle.
Significance: TRIC-A channels may have unexplained roles in store Ca^{2+} distribution but provide a potential pharmaceutical target for vasomodulation.

The TRIC channel subtypes, namely TRIC-A and TRIC-B, are intracellular monovalent cation-specific channels and likely mediate counterion movements to support efficient Ca^{2+} release from the sarco/endoplasmic reticulum. Vascular smooth muscle cells (VSMCs) contain both TRIC subtypes and two Ca^{2+} release mechanisms; incidental opening of ryanodine receptors (RyRs) generates local Ca^{2+} sparks to induce hyperpolarization and relaxation, whereas agonist-induced activation of inositol trisphosphate receptors produces global Ca^{2+} transients causing contraction. *Tric-a* knock-out mice develop hypertension due to insufficient RyR-mediated Ca^{2+} sparks in VSMCs. Here we describe transgenic mice overexpressing TRIC-A channels under the control of a smooth muscle cell-specific promoter. The transgenic mice developed congenital hypotension. In *Tric-a*-overexpressing VSMCs from the transgenic mice, the resting membrane potential decreased because RyR-mediated Ca^{2+} sparks were facilitated and cell surface Ca^{2+}-dependent K^+ channels were hyperactivated. Under such hyperpolarized conditions, L-type Ca^{2+} channels were inactivated, and thus, the resting intracellular Ca^{2+} levels were reduced in *Tric-a*-overexpressing VSMCs. Moreover, *Tric-a* overexpression impaired inositol trisphosphate-sensitive stores to diminish agonist-induced Ca^{2+} signaling in VSMCs. These altered features likely reduced vascular tonus leading to the hypotensive phenotype. Our *Tric-a*-transgenic mice together with *Tric-a* knock-out mice indicate that TRIC-A channel density in VSMCs is responsible for controlling basal blood pressure at the whole-animal level.

Two major classes of intracellular Ca^{2+} channels, inositol 1,4,5-trisphosphate receptors (IP_3Rs)[3] and ryanodine receptors (RyRs), provide the fundamental pathway for Ca^{2+} release from internal stores into the cytoplasm (1–4). IP_3R-mediated Ca^{2+} release from IP_3-sensitive stores in the sarco/endoplasmic reticulum (SR/ER) plays a central role in cellular signaling systems. RyR-mediated Ca^{2+} release from caffeine-sensitive stores also regulates important cellular functions such as excitation-contraction coupling, secretion/exocytosis, and gene expression, primarily in excitable cells. When the divalent cation Ca^{2+} is released from the SR/ER, a negative potential is likely generated on the luminal side and may inhibit subsequent Ca^{2+} release. Therefore, counterion movements may balance SR/ER membrane potential to establish efficient Ca^{2+} release mechanisms in various cell types (5, 6). Indeed, previous electrophysiological and fluorometric analyses detected several ionic currents, such as K^+, Cl^-, and H^+ fluxes, across the SR/ER membrane (7–10). However, the channel/transporter components mediating such ionic flows have not been identified, and thus, their contributions to the proposed counterion movements are largely unknown.

Recently, we identified two TRIC (trimeric intracellular cation) channel subtypes, TRIC-A and TRIC-B, that assemble into bullet-shaped homotrimers to form monovalent cation-selective channels in the SR/ER and nuclear membranes (11–13). Double-knock-out mice lacking both the *Tric-a* and *Tric-b* genes show embryonic cardiac failure, and the mutant car-

* This work was supported in part by grants from the Ministry of Education, Culture, Sports, Science, and Technology of Japan (Grants-in-Aid for Scientific Research and Platform for Drug Design, Discovery, and Development), the Ministry of Health, Labour and Welfare, the Vehicle Racing Commemorative Foundation, the Astellas Foundation, the Suzuken Memorial Foundation, the Kanae Foundation, the Japan Foundation for Applied Enzymology, the Takeda Science Foundation, the Ono Medical Research Foundation, and the Kowa Life Science Foundation.
[S] This article contains supplemental Figs. S1—S4.
[1] Both authors contributed equally to this work.
[2] To whom correspondence should be addressed: Dept. of Biological Chemistry, Graduate School of Pharmaceutical Sciences, Kyoto University, Kyoto 606-8501, Japan. Tel.: 81-75-753-4572; Fax: 81-75-753-4605; E-mail: takeshim@pharm.kyoto-u.ac.jp.

[3] The abbreviations used are: IP_3R, inositol trisphosphate (IP_3) receptor; BK channel, big-conductance Ca^{2+}-dependent K^+ channel; CPA, cyclopiazonic acid; ER, endoplasmic reticulum; PE, phenylephrine; RyR, ryanodine receptor; STOC, spontaneous transient outward current; SR, sarcoplasmic reticulum; SMC, smooth muscle cell; VSMC, vascular smooth muscle cell.

diomyocytes display weak RyR-mediated Ca^{2+} release from the SR (14). *Tric-a* knock-out mice develop hypertension associated with vascular hypertonicity, and the mutant vascular smooth muscle cells (VSMCs) show insufficient Ca^{2+} sparks for inducing hyperpolarization (15). Moreover, mutant skeletal muscle from *Tric-a* knock-out mice occasionally exhibits alternan contraction responses, likely due to destabilized RyR-mediated Ca^{2+} release (16). On the other hand, *Tric-b* knock-out mice develop respiratory failure at birth, and the mutant alveolar epithelial cells exhibit compromised IP_3R-mediated Ca^{2+} release and insufficient handling of surfactant lipids (17). These defects observed in the knock-out mice support our hypothesis that TRIC channel subtypes partly mediate counterion movements to facilitate SR/ER Ca^{2+} release.

VSMCs possess both caffeine- and IP_3-sensitive stores and also contain both TRIC-A and TRIC-B channels. Therefore, VSMCs are an ideal model system to examine the physiological functions of TRIC channel subtypes. We recently detected not only insufficient RyR-mediated Ca^{2+} sparks but also facilitated IP_3R-mediated Ca^{2+} transients in *Tric-a* knock-out VSMCs (15). These observations led to the hypothesis that TRIC-A channels preferentially support RyR-mediated Ca^{2+} release and also regulate Ca^{2+} distribution between the caffeine- and IP_3-sensitive stores. To further verify this hypothesis, we planned to generate mutant mice carrying the SMC-specific *Tric-a* transgene and to examine altered features in *Tric-a*-overexpressing VSMCs.

EXPERIMENTAL PROCEDURES

Transgenic Mice and Blood Pressure Monitoring—Transgenic mice overexpressing TRIC-A channels under the control of the human α-smooth muscle actin promoter were generated and genotyped as previously described (15). The transgenic and wild-type littermates (8–12 weeks old) were examined physiologically and biochemically in this study. All experiments were conducted with the approval of the Animal Research Committee at Kyoto University according to the regulations on animal experimentation at Kyoto University. To telemetrically monitor arterial blood pressure, PA-C10 transmitters (Data Sciences International, New Brighton, MN) were implanted into mice, and the pressure-sensing catheters were inserted into the aortic arch under anesthesia. Radio signals from the implanted transmitter were captured using the Physiotel RPC-1 receiver (Data Sciences International), and the data were stored online using the Dataquest ART data acquisition system (Data Sciences International). Blood pressure and heart rate in the conscious state were also monitored by tail-cuff plethysmography (Model BP-98A-L, Softron) during the daytime.

Anatomical Analysis—Histological and ultrastructural analyses were carried out as described previously (18). Briefly, mesenteric arteries from adult mice were fixed in 3% paraformaldehyde, 2.5% glutaraldehyde, and 0.1 M sodium cacodylate, pH 7.4. After the tissues were dehydrated and embedded in Epon, ultrathin sections (~80 nm thick) were prepared and stained with toluidine blue for histological observation or uranyl acetate and lead citrate for electron microscopic analysis (JEM-200CX, JEOL).

Imaging Analysis—Single VSMCs were enzymatically isolated from mesenteric arteries and subjected to Ca^{2+} spark and membrane potential monitoring as described previously (15, 19). Briefly, single VSMCs were seeded onto glass-bottomed dishes and incubated with 5 μM Fluo-4AM (Dojindo) in HEPES-buffered saline: 137 mM NaCl, 5.9 mM KCl, 2.2 mM $CaCl_2$, 1.2 mM $MgCl_2$, 14 mM glucose, and 10 mM HEPES, pH 7.4, with NaOH). The Ca^{2+} spark images with excitation at 488 nm and emission at >520 nm were captured using a total internal reflection fluorescence microscopy system (TE-2000U, Nikon), and the data were analyzed using the custom software Aquacosmos (Hamamatsu Photonics). For membrane potential monitoring, single VSMCs on glass-bottomed dishes were perfused with HEPES-buffered saline containing 200 nM oxonol VI (Fluka). Fluorescence images with excitation at 559 nm and emission at >606 nm were captured at a sampling rate of ~1.6 s using a confocal microscope system (FV1000, Olympus).

For monitoring intracellular Ca^{2+} concentration ($[Ca^{2+}]_i$) in VSMCs, the inner surface of the artery was gently wiped with gauze to remove endothelial cells as described previously (20). The resulting arterial muscle segments were incubated with 5 μM Fura-PE3AM (Santa Cruz) and 0.02% cremophor EL (Sigma) and tightly fixed with fine steel pins onto a silicone rubber sheet, which was placed on a glass-bottomed dish. A CCD camera (ImagEM, Hamamatsu Photonics) mounted on the microscope (DMI 4000B, Leica) equipped with a polychromatic illumination system (MetaFluor ver7.7r3, Molecular Device) was used to capture fluorescence images with excitation at 340 and 380 nm and emission at >510 nm at room temperature (~23 °C).

Patch Clamp and Membrane Potential Recording—Whole-cell voltage clamp recording was carried out using the Axopatch 200B amplifier (Molecular Device) essentially as described previously (21). For spontaneous transient outward current (STOC) monitoring in single VSMCs, the STOC pipette solution (140 mM KCl, 4 mM $MgCl_2$, 5 mM Na_2ATP, 0.05 mM EGTA, and 10 mM HEPES, pH 7.2, with KOH) and HEPES-buffered saline as a bathing solution were utilized. For the recording of total Ca^{2+}-dependent K^+ currents, the BK pipette solution (140 mM KCl, 1 mM $MgCl_2$, 6.1 mM $CaCl_2$, 1 mM Na_2ATP, 10 mM EGTA, and 10 mM HEPES, pH 7.2, with KOH, *p*Ca 6.5) and HEPES-buffered saline containing 100 μM $CdCl_2$ as a bathing solution were utilized. All physiological measurements were carried out at room temperature.

The arterial muscle segments were subjected to transmembrane potential monitoring with high resistance glass microelectrodes (30–50 megaohms) filled with 3 M KCl solution as described previously (22). Membrane potential was determined as an average of the potentials obtained from stable impalements longer than 1 min from different areas in the muscle segment. The transmembrane potential was amplified by a high-input impedance amplifier with capacitance neutralization (MEZ-7200, Nihon Kohden), and the electrical signals were digitized and analyzed using a Power Lab system (AD Instruments). The bath solution used was modified Krebs solution babbled with 95% O_2, 5% CO_2 and maintained at 37 °C at pH ~ 7.4 (112 mM NaCl, 4.7 mM KCl, 2.2 mM $CaCl_2$, 1.2 mM $MgSO_4$, 25 mM $NaHCO_3$, 1.2 mM KH_2PO_4, and 14 mM glucose).

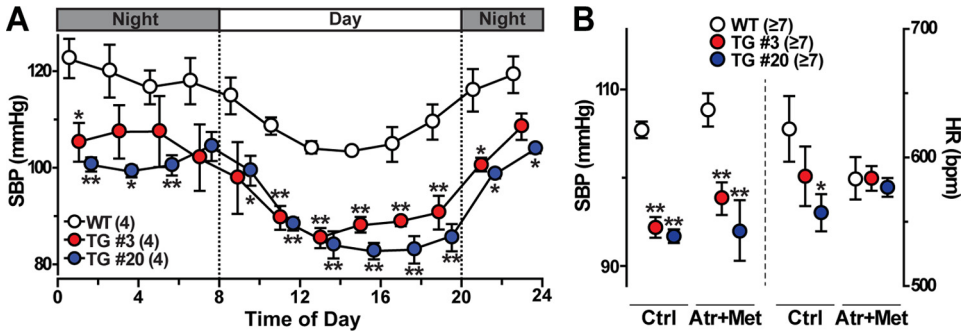

FIGURE 1. **Hypotension in SMC-specific *Tric-a*-transgenic mice.** *A*, telemetric blood pressure monitoring is shown. Circadian fluctuations in systolic blood pressure (*SBP*) were monitored, and the data were averaged over each 2-h interval during a 24-h period. *B*, systolic blood pressure and heart rate (*HR*) monitoring by tail-cuff plethysmography during the daytime. After the base-line monitoring (*Ctrl*), autonomic controls were blocked using an intraperitoneal injection of the muscarinic antagonist atropine (*Atr*, 4 mg/kg) and the β-antagonist metoprolol (*Met*, 4 mg/kg). Upon drug application, HR was quickly attenuated, but systolic blood pressure changed in a time-dependent manner (see supplemental Fig. S1*E*). The data represent the mean ± S.E., and the numbers of mice examined are shown in *parentheses*. Significant differences between the genotypes are marked with asterisks (*, $p < 0.05$; **, $p < 0.01$ by Student's *t* test).

RT-PCR and Immunochemical Analysis—For quantitative PCR analysis, total RNA preparations from various tissues (at least three mice of each genotype) were used as templates for cDNA synthesis (ReverTra ACE qPCR-RT kit, Toyobo) and analyzed using a real-time PCR system according to the manufacturer's instructions (Thermal Cycler TP800, Takara). The cycle threshold was determined from the cDNA amplification curve as an index for relative mRNA content in each reaction. The PCR primer sets used in this study were listed previously (15). For immunochemical analysis, tissue lysates and fixed VSMCs were examined using primary antibodies to TRIC channel subtypes and calnexin (Santa Cruz) as described previously (14, 18).

RESULTS

Hypotension in SMC-specific Tric-a-Transgenic Mice—We previously generated transgenic mice with SMC-specific overexpression of TRIC-A channels using the α-smooth muscle actin promoter (23). Although the constructed *Tric-a*-transgene rescues the hypertensive phenotype developed in *Tric-a* knock-out mice (15), the effects of the transgene have not been examined in a wild-type genetic background. Therefore, we generated two *Tric-a*-transgenic mouse lines in wild-type backgrounds, which we designated as TgA3 and TgA20 mice. Both transgenic mouse lines grew and reproduced normally (supplemental Fig. S1*A*). RT-PCR analysis demonstrated that the transgene was highly expressed in blood vessels and other tissues containing SMCs, and its expression was faintly detected in the liver and skeletal muscle (supplemental Fig. S1*B*). In accordance with our previous observation that the transgene dosage in the TgA20 mouse line is higher than in the TgA3 line (15), TgA20 mice showed higher transgene expression in SMC-containing tissues than TgA3 mice in RT-PCR analysis (supplemental Fig. S1*C*).

By telemetric blood pressure monitoring, both TgA20 and TgA3 mice, even at a young-adult age, showed low blood pressure levels throughout the entire day (Fig. 1*A*). This hypotensive phenotype was further confirmed by tail-cuff monitoring (Fig. 1*B*). Most likely reflecting the difference in transgene expression between the mouse lines, TgA20 mice developed slightly lower blood pressure than TgA3 mice. Elevated blood pressure stimulates the baroreceptor reflex and effectively decreases heart rate in normal animals (24). However, in both transgenic mice, a slow heart rate was clearly observed under hypotensive conditions. The blockage of cardiac autonomic controls by coapplication of the muscarinic blocker atropine and the β-adrenoreceptor blocker metoprolol ameliorated the bradycardic phenotype, whereas low blood pressure was clearly maintained in the transgenic mice (Fig. 1*B*). Therefore, ectopic *Tric-a* expression in baroreceptors and/or autonomic neurons likely produced vagal-dominant states in both transgenic mice. Moreover, the α1-adrenoreceptor blocker prazosin induced similar vasodilating effects in both wild-type and transgenic mice (supplemental Fig. S1*E*). These observations suggest that impaired sympathetic stimuli to the heart and vascular smooth muscle were not significant contributors to hypotension in the transgenic mice. It may be reasonable that altered vascular functions underlie the hypotensive phenotype in both transgenic mice because *Tric-a* knock-out mice develop hypertension due to increased vascular tonus (15).

Tric-a-Overexpressing VSMCs from the Transgenic Mice—Resistance arteries distributed to peripheral tissues are primarily responsible for blood pressure maintenance. The mesenteric artery is a typical resistance vessel and was examined in our studies below. By RT-PCR analysis of mesenteric arteries, the *Tric-a* mRNA levels in TgA20 and TgA3 mice were at least 400-fold greater than those of wild-type controls (Fig. 2*A*). Western blot analysis confirmed *Tric-a* overexpression, and enhanced immunoreactivities provided estimates that the TRIC-A protein levels in the arteries from the transgenic mice were increased more than 500-fold compared with wild-type arteries (Fig. 2*B*). However, neither the heart nor skeletal muscle from the transgenic mice showed an obvious enhancement of TRIC-A immunoreactivity (supplemental Fig. S1*D*). Such SMC-specific overexpression of TRIC-A channels may not cause serious damage to the fundamental functions of resistance arteries because the transgenic mice retained circadian blood pressure variation (Fig. 1*A*) and regular blood pressure fluctuation in response to typical vasodilators targeting VSMCs (supplemental Fig. S1*E*).

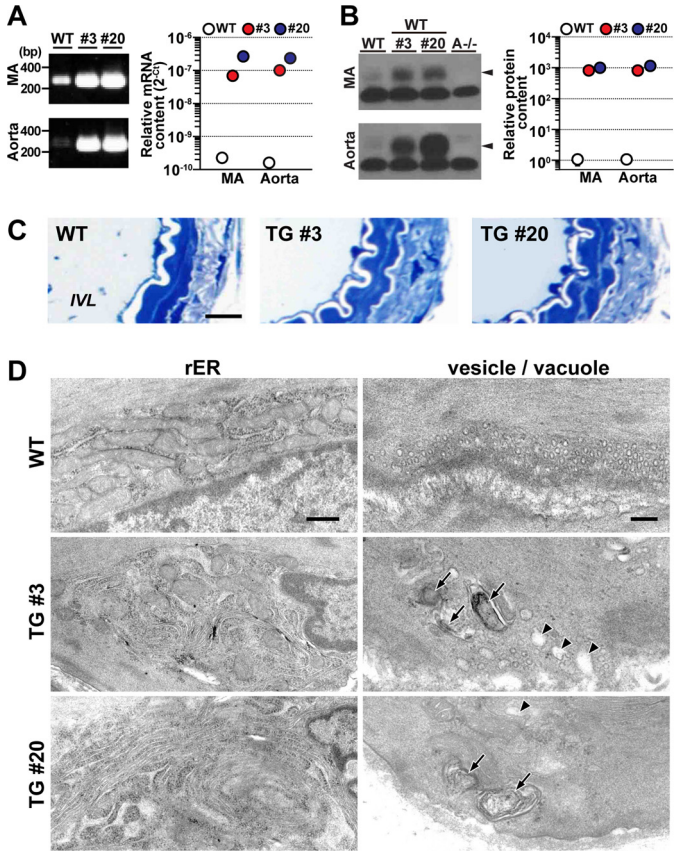

FIGURE 2. **Irregular membranous features of *Tric-a*-overexpressing VSMCs.** *A*, shown is quantitative detection of *Tric-a* mRNA in mesenteric artery (*MA*) and aorta. Total tissue RNA preparations from transgenic (#3 and #20) and wild-type mice ($n = 3$) were examined by quantitative RT-PCR using a primer set for amplifying *Tric-a* mRNA from both the endogenous gene and the transgene. The cDNA fragments amplified by 33 PCR cycles were analyzed by agarose gel electrophoresis. RT-PCR data obtained are summarized in the *right graph*. The cycle threshold (*Ct*) indicates the cycle number at which the amount of amplified cDNA reached a fixed threshold in each reaction. *B*, Western blot analysis of TRIC-A protein in MA and aorta is shown. The vessels dissected from the *Tric-a*-transgenic (*#3* and *#20*), *Tric-a* knock-out (*A*−/−), and wild-type mice were homogenized to prepare total cell lysates (post-nuclear fractions). Wild-type lysates (10 μg of protein) with or without lysates from the transgenic mice (0.1 μg) were analyzed with an antibody against the TRIC-A protein. Lysates from the *Tric-a* knock-out mice (10 μg) served as negative controls. *Arrowheads* indicate TRIC-A protein bands. Immunoreactive signals were digitalized and statistically analyzed to estimate the relative contents of TRIC-A protein in the different genotypes as shown in the *right graph*. *C*, normal histology in MA from *Tric-a*-transgenic mice is shown. Mesenteric artery preparations were incubated in a Ca^{2+}-free solution for ~20 min and then fixed for anatomical analysis. Thin sections were stained with toluidine blue for photomicroscopic observation. *IVL*, intravascular lumen. *Scale bar*, 10 μm. *D*, shown is formation of stacked ER elements and vacuoles in *Tric-a*-overexpressing VSMCs. Rough ER (*rER*) elements at the cell-interior portion (*left panels*: *scale bar*, 500 nm) are shown. Stacks of rough ER elements were frequently observed in VSMCs from transgenic mice (~27% of TgA3 cells and 80% of TgA20 cells), whereas such stacked ER was not detected in wild-type controls ($n = 45$–97 cells from 3–6 mice in each genotype). Surface vesicles and vacuoles were located at the cell periphery (*right panels*: *scale bar*, 200 nm). TRIC-A overexpression appeared to promote the formation of large-sized vacuoles containing myelin figures (*arrows*) or no electron-dense materials (*arrowheads*). Such vacuoles were frequently observed in >50% of VSMCs from TgA3 and TgA20 mice but only detected in 9.5% of wild-type VSMCs ($n = 53$–89 cells from 6 mice in each genotype).

Histological observations revealed no obvious abnormalities in mesenteric arteries from TgA20 and TgA3 mice (Fig. 2*C*). For example, under relaxation conditions after incubation in a Ca^{2+}-free bathing solution, similar passive diameters and VSMC layer thicknesses of the arteries were observed in the transgenic and wild-type mice (supplemental Fig. S2*A*). These observations suggest that the hypotensive phenotype was mainly caused by insufficient myogenic tonus of resistance arteries under *in vivo* conditions in the transgenic mice.

Electron microscopic observation detected irregular membranous ultrastructures in mesenteric arteries from the transgenic mice. In *Tric-a*-overexpressing VSMCs, stacked rough ER elements accumulated around cell-interior regions (Fig. 2*D*, *left panels*). The generation of stacked rough ER has been repeatedly reported in various cell types overexpressing integral SR/ER membrane proteins (25, 26), and such irregular ER elements were not detected in wild-type VSMCs. Indeed, dense immunofluorescence signals of ectopic TRIC-A channels were predominantly observed in the cell-interior regions of VSMCs from transgenic mice (supplemental Fig. S2*B*), suggesting that the ER stacks were generated by nonspecific effects of excess TRIC-A protein. In SMCs, IP_3Rs are distributed uniformly over the nuclear and ER/SR membranes (27, 28), whereas RyRs are predominantly localized in peripheral SR elements (29, 30). Therefore, it is possible that the formation of the stacked rough ER may have a functional impact on IP_3-sensitive stores. However, such a morphological abnormality may minimally affect caffeine-sensitive stores.

In VSMCs, free-floating small vesicles, originally referred to as "surface vesicles" (31), were abundantly arranged underneath the cell membrane (Fig. 2*D*, *right panels*). Accompanied by the surface vesicles, larger-sized vacuoles with myelin figures (multilamellar lipid deposits) or without electron-dense material in the lumen were frequently observed in *Tric-a*-overexpressing VSMCs. Such vacuoles were rarely detected in wild-type VSMCs. To resolve the stacked ER elements, the large vacuoles may be aberrantly generated in *Tric-a*-overexpressing VSMCs. Alternatively, the excess amounts of TRIC-A protein may have promoted the swelling and fusion of normal small vesicles, generating the vacuoles. Swelling of SR elements is frequently accompanied by stored Ca^{2+} overloading in skeletal and cardiac muscle (16, 32, 33), and RyR-mediated Ca^{2+} sparks are predominantly generated underneath the cell membrane in VSMCs (3, 4). The facilitated formation of the vacuoles may imply altered Ca^{2+}-handling characteristics in caffeine-sensitive stores of *Tric-a*-overexpressing VSMCs.

Facilitated Hyperpolarization Signaling in Tric-a-Overexpressing VSMCs—In VSMCs, incidental activation of RyRs generates Ca^{2+} sparks and then activates big-conductance Ca^{2+}-dependent K^+ (BK) channels to evoke STOCs, leading to hyperpolarization (3, 4). To identify the direct cause of the hypotensive phenotype, we investigated Ca^{2+} spark and STOC generation in VSMCs from the transgenic mice because hyperpolarization signaling is impaired in *Tric-a* knock-out VSMCs (15). Our Ca^{2+} spark imaging captured hyperactivated sparks at specified intracellular hotspots in single VSMCs prepared from the transgenic mice (Fig. 3*A*). Statistical analysis of the imaging data detected no difference in Ca^{2+} spark amplitude between the genotypes. However, Ca^{2+} spark frequency was substantially elevated, and the number of spark hotspots was significantly increased in *Tric-a*-overexpressing VSMCs from both TgA20 and TgA3 mice (Fig. 3, *B*–*D*). RT-PCR analysis detected no altered gene expression of the key components in

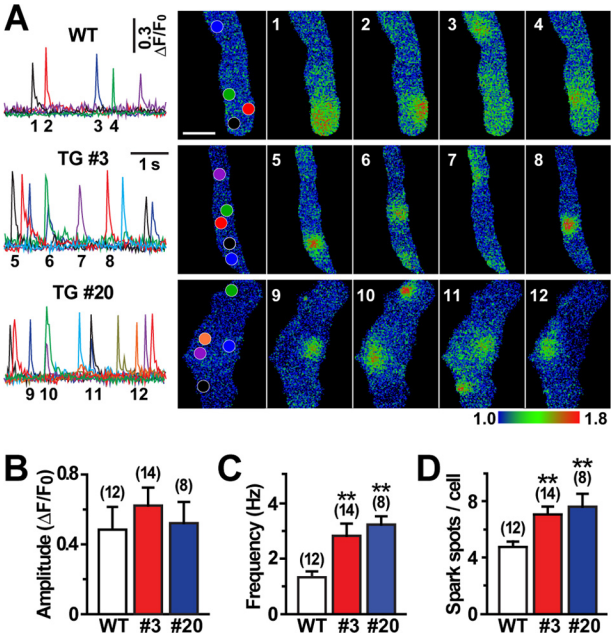

FIGURE 3. **Facilitated Ca^{2+} sparks in *Tric-a*-overexpressing VSMCs.** Single VSMCs were prepared from mesenteric arteries and loaded with Fluo-4 for total internal reflection fluorescence imaging. *A*, shown are representative Ca^{2+}-spark monitoring data in a normal bathing solution. The fluorescence intensity was normalized to the base-line intensity to yield the relative intensity (F/F_0), and time courses of the intensity changes at the subcellular hotspots (see *colored circles* in the F_0 cell images) are illustrated in the traces (*scale bar*, 5 μm). The F/F_0 images were color-coded as indicated by the *bar* to prepare the Ca^{2+}-spark images at the numbered time points. The data on spark amplitude (*B*), frequency (*C*), and spot number (*D*) are summarized for each genotype. Significant differences between the genotypes are indicated by asterisks (**, $p < 0.01$ by *t* test).

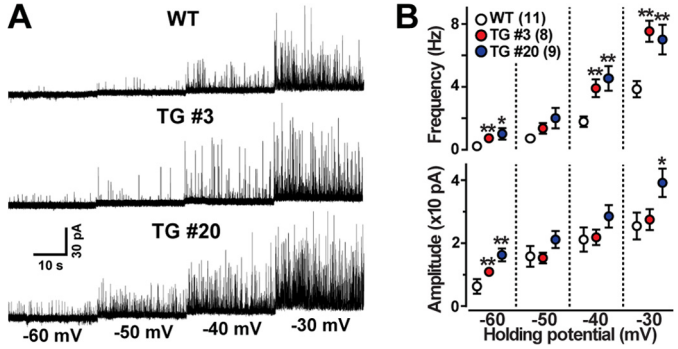

FIGURE 4. **Facilitated STOCs in *Tric-a*-overexpressing VSMCs.** The membrane potential of single VSMCs was controlled by the whole-cell patch clamp technique using the STOC pipette to monitor membrane currents. Representative STOC recording data are illustrated in *A*. The data for STOC frequency and amplitude are summarized in *B*. The data represent the mean ± S.E., and the numbers of cells examined from at least three mice are shown in *parentheses*. Significant differences between the genotypes are indicated by asterisks (*, $p < 0.05$; **, $p < 0.01$ by *t* test).

intracellular Ca^{2+} signaling and G protein-coupled receptor signaling, such as RyR, IP_3R, Ca^{2+}-pump protein, α-adrenoreceptor, and phospholipase C, in mesenteric arteries and thoracic aorta from the transgenic mice (supplemental Fig. S3*A*). Therefore, *Tric-a* overexpression appears to hyperactivate Ca^{2+} spark generation without affecting the cellular levels of major Ca^{2+}-handling proteins in VSMCs.

For monitoring BK channel-mediated STOCs, single VSMCs were examined by patch clamp recording using the nominally Ca^{2+}-free STOC pipette solution. VSMCs from the transgenic mice showed highly activated STOCs (Fig. 4*A*). In particular, both STOC frequency and amplitude were markedly increased at a holding potential of −60 mV near the resting potential in the *Tric-a*-overexpressing cells (Fig. 4*B*). We also monitored total K^+ currents using the Ca^{2+}-containing BK pipette solution and examined the effects of the BK channel inhibitor iberiotoxin on VSMCs. VSMCs from the transgenic mice showed normal levels of total K^+ currents both sensitive and insensitive to iberiotoxin (supplemental Fig. S3*B*). Therefore, despite normal cell-surface densities of BK channels, STOC generation was likely facilitated under physiological conditions in *Tric-a*-overexpressing VSMCs. The enhanced STOCs were fully consistent with the hyperactivated Ca^{2+} sparks observed (Fig. 3), suggesting that hyperpolarization signaling generated by functional cross-talk between the RyR and BK channels was stimulated in VSMCs from the transgenic mice.

Deepened Resting Potential in Tric-a-Overexpressing VSMCs—In SMCs, BK channel-mediated STOCs contribute to the maintenance of resting membrane potential and the fine-tuning of cellular excitability (3, 4). Based on the facilitated STOCs observed, we next focused on membrane potential in *Tric-a*-overexpressing VSMCs and leveraged confocal microscopic imaging using the voltage-dependent dye oxonol VI. Imaging analysis showed that fractional fluorescence intensity was clearly decreased in VSMCs from both TgA20 and TgA3 mice at basal conditions (Fig. 5*A*). The decreased intensities suggested that *Tric-a*-overexpressing VSMCs were deeply hyperpolarized during the resting state (Fig. 5*B*). We previously prepared the calibration plot representing the relationship between the fluorescence intensity and membrane potential using the reported resting potential of −59.9 mV in wild-type VSMCs (15, 34). The calibration plot estimated that the resting membrane potentials of TgA3, TgA20, and *Tric-a* knock-out VSMCs were −63.6, −63.9, and −54.6 mV, respectively. The estimated potentials agreed closely with actual measurement values from direct monitoring using high resistance microcapillary electrodes; the detected resting potentials of wild-type, TgA20, and *Tric-a* knock-out VSMCs were −59.4 ± 0.6, −64.8 ± 1.0, and −53.7 ± 0.7 mV, respectively (supplemental Fig. S3*C*). Moreover, from oxonol VI imaging, enlarged intensity shifts were evoked by iberiotoxin in VSMCs from the transgenic mice (Fig. 5*C*). The enhanced responses directly reflected the hyperactivation of BK channels at resting conditions in *Tric-a*-overexpressing VSMCs. However, while being exposed to iberiotoxin, similar fractional intensities were observed in wild-type and *Tric-a*-overexpressing VSMCs. Because many channels and transporters, in addition to BK channels, contribute to generating resting potential, the iberiotoxin-induced realignment of resting intensities suggested that the components other than BK channels functioned normally on the cell surface of *Tric-a*-overexpressing VSMCs. In summary, these results suggest that specific hyperactivation of BK channels lowered resting membrane potential in VSMCs from the transgenic mice.

Altered Ca^{2+} Handling in Tric-a-Overexpressing VSMCs—Of the excitable cell types, SMCs have relatively shallow resting membrane potentials. In VSMCs at basal conditions, L-type voltage-gated Ca^{2+} channels generate persistent Ca^{2+} influx

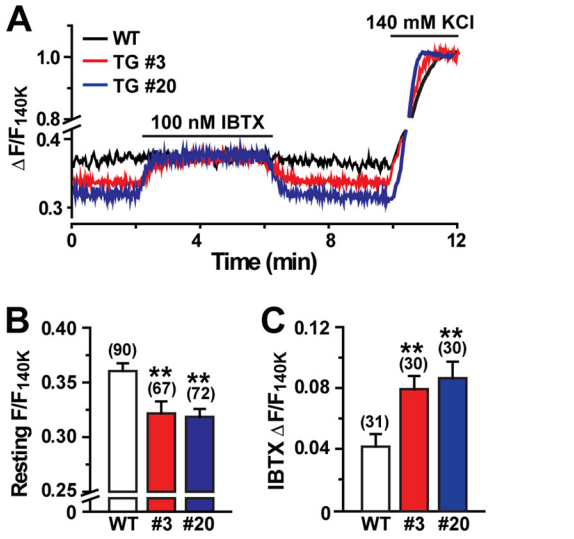

FIGURE 5. **Decreased resting membrane potential in *Tric-a*-overexpressing VSMCs.** Single VSMCs were examined by confocal microscopic imaging using the voltage-dependent dye oxonol VI. Cellular fluorescence intensities were normalized to the maximum value to yield the fractional intensity (F/F_{140K}). *A*, shown are representative imaging data. *B*, shown are the summarized data of the resting intensity. *C*, shown are the summarized data of the intensity shift by iberiotoxin (*IBTX*). The data represent the mean ± S.E., and the numbers of cells examined from at least three mice are shown in *parentheses*. Significant differences between the genotypes are indicated by asterisks (**, $p < 0.01$ by *t* test).

and maintain both resting $[Ca^{2+}]_i$ and intrinsic tonus (3, 4). We examined cellular Ca^{2+} handling in VSMCs from the transgenic mice and found several abnormal features. First, our ratiometric Fura-PE3 imaging detected that resting $[Ca^{2+}]_i$ was markedly decreased in VSMCs from the transgenic mice (Fig. 6, *A* and *B*). In accordance with the detected membrane potentials, TgA20 cells exhibited slightly lower $[Ca^{2+}]_i$ than TgA3 cells. In a Ca^{2+}-free extracellular solution, similar resting $[Ca^{2+}]_i$ levels were observed in wild-type and *Tric-a*-overexpressing VSMCs. Moreover, the downward-adjusted resting $[Ca^{2+}]_i$ was clearly rescued by the L-type Ca^{2+} channel inhibitor verapamil and the activator BayK8644 in *Tric-a*-overexpressing VSMCs (Fig. 6*C*). Therefore, L-type Ca^{2+} channels were likely inactivated at basal conditions, and resting $[Ca^{2+}]_i$ was thus decreased in *Tric-a*-overexpressing VSMCs.

VSMCs contain both IP_3- and caffeine-sensitive stores, and they are functionally interconnected (3, 4). The SR/ER Ca^{2+}-pump inhibitor cyclopiazonic acid (CPA) causes Ca^{2+} leakage from both stores, and the total stored Ca^{2+} contents can be estimated from CPA-induced responses. CPA-induced Ca^{2+} depletion from intracellular stores generally triggers store-operated Ca^{2+} entry (35). VSMCs from the transgenic mice exhibited normal CPA-induced and store-operated Ca^{2+} entry responses (Fig. 6, *D* and *E*). However, *Tric-a*-overexpressing VSMCs showed weak IP_3R-mediated Ca^{2+} release in response to the α-adrenoreceptor agonist phenylephrine (*PE*) (Fig. 6, *F* and *G*). We also observed that PE-induced responses were diminished after normal caffeine-evoked transients in *Tric-a*-overexpressing VSMCs (supplemental Fig. S4*A*). Furthermore, in response to sequential applications of PE and caffeine under Ca^{2+}-free conditions, *Tric-a*-overexpressing VSMCs exhibited poor IP_3R-mediated transients immediately followed by enhanced RyR-mediated transients (Fig. 6, *H* and *I*). It is unlikely that poor PE-induced transients were due to compromised phosphoinositide turnover signaling because RT-PCR analysis suggested normal expression of major components of adrenoreceptor-mediated signaling in *Tric-a*-overexpressing VSMCs (supplemental Fig. S3*A*). Therefore, in addition to facilitating Ca^{2+} spark generation as described above, *Tric-a* overexpression appeared to affect IP_3-sensitive stores in VSMCs.

DISCUSSION

Single-channel recording in planar lipid bilayers demonstrated that purified TRIC-A and TRIC-B proteins form monovalent cation-specific channels (12–14). Therefore, TRIC channel subtypes likely function as SR/ER K^+ channels under intracellular conditions. Although TRIC channels exhibit marked voltage dependence, they are likely to contribute to persistent K^+ flux when membrane potential and osmotic pressure fluctuate in the SR/ER (11). In our previous study, *Tric-a* knock-out mice displayed high vascular tonus and developed hypertension because the hyperpolarization signaling triggered by Ca^{2+} sparks was compromised in the knock-out VSMCs (15). In the present study, as a polar opposite of the TRIC-A-null model, SMC-specific *Tric-a*-transgenic mice developed hypotension, and Ca^{2+} spark generation was facilitated in *Tric-a*-overexpressing VSMCs. Therefore, we reasonably conclude that TRIC-A channels support RyR-mediated Ca^{2+} spark generation and contribute to setting the basal tonus in VSMCs. From a biophysical point of view, the density-dependent contribution of TRIC-A channels to Ca^{2+} spark generation can be explained by an oversimplified scheme (supplemental Fig. S4*B*). Several lines of evidence indicate that RyR subtypes are nonselective cation channels equipped with large diameter pores and can bidirectionally conduct Ca^{2+} and K^+ (36). Our model tentatively assumes that only K^+ provided by TRIC-A or RyR channels acts as a counter ion for stabilizing SR membrane potential during Ca^{2+} release. In wild-type VSMCs, both TRIC-A and RyR channels may conduct counter-K^+ to support Ca^{2+} release. However, the SR K^+ currents are likely insufficient to stabilize membrane potential during vital Ca^{2+} release, and many events of incidental RyR opening may fail to grow to the Ca^{2+} sparks visualized in Ca^{2+}-imaging analysis. Even lower SR K^+ currents are proposed for *Tric-a* knock-out VSMCs, and thus, the growth to detectable Ca^{2+} sparks is further attenuated by the TRIC-A-null conditions. In contrast, in *Tric-a*-overexpressing VSMCs, enhanced SR K^+ currents may no longer attenuate the growth of Ca^{2+} sparks. Additionally, the excess K^+ currents mediated by overexpressed TRIC-A channels may persistently prevent negative-shifting of the membrane potential toward the Ca^{2+} reversal potential and could effectively maintain Ca^{2+} release from partially depleted stores. Such biophysical mechanisms likely underlie the facilitated Ca^{2+} sparks observed in *Tric-a*-overexpressing VSMCs. In the present study, several altered functions linked to the hypotensive phenotype were characterized in *Tric-a*-overexpressing VSMCs (Fig. 7). Excess TRIC-A channels facilitate Ca^{2+} spark (Fig. 3) and STOC generation (Fig. 4) and decrease resting membrane potential in VSMCs (Fig. 5). Under such

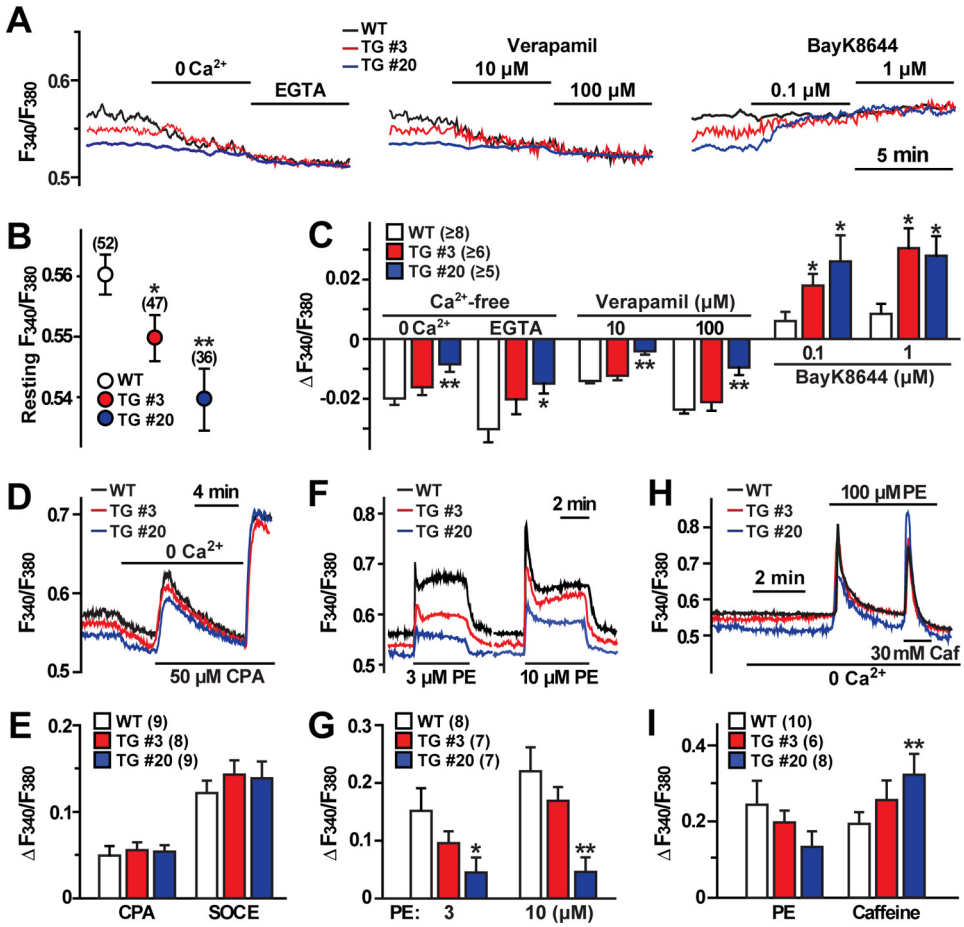

FIGURE 6. **Abnormal Ca^{2+} handling in *Tric-a*-overexpressing VSMCs.** VSMC segments were examined by Fura-PE3 Ca^{2+} imaging. The change in $[Ca^{2+}]_i$ was expressed as ratio of the fluorescence intensity (F_{340}/F_{380}). *A–C*, shown is decreased resting $[Ca^{2+}]_i$ in *Tric-a*-overexpressing VSMCs. *A*, representative traces under normal conditions and responses to Ca^{2+} removal and L-type Ca^{2+} channel modulators are illustrated. Resting $[Ca^{2+}]_i$ data are summarized in *B*, and $[Ca^{2+}]_i$ responses are analyzed in *C*. *D* and *E*, normal Ca^{2+} store contents in *Tric-a*-overexpressing VSMCs are shown. Representative CPA-induced responses are shown in *D*, and the data are summarized in *E*. *F* and *G*, impaired IP_3-mediated Ca^{2+} release in *Tric-a*-overexpressing VSMCs . Representative PE-induced responses are shown in *F*, and the data are summarized in *G*. *H* and *I*, altered Ca^{2+} distribution to store compartments in *Tric-a*-overexpressing VSMCs are shown. Sequential responses to PE and caffeine (*Caf*) under Ca^{2+}-free conditions are shown in (*H*), and the data are summarized in (*I*). The data represent the mean ± S.E., and the numbers of mice examined are shown in *parentheses*. Significant differences between the genotypes are indicated by *asterisks* (*, $p < 0.05$; **, $p < 0.01$ by *t* test).

hyperpolarized conditions, L-type Ca^{2+} channels are relatively inactivated, and resting $[Ca^{2+}]_i$ is suppressed in *Tric-a*-overexpressing VSMCs (Fig. 6). Decreased $[Ca^{2+}]_i$ in VSMCs likely reduces the intrinsic tonus of resistance arteries, leading to hypotension in the *Tric-a*-transgenic mice (Fig. 1).

VSMCs possess both caffeine- and IP_3-sensitive stores and contain both TRIC-A and TRIC-B channels with similar estimated expression levels (15). In accordance with previous studies (37–39), our Ca^{2+} imaging also detected that caffeine-induced responses were larger than agonist-induced responses in wild-type VSMCs from mesenteric arteries (Fig. 6*H*). In addition to the altered features directly linked to hypotension, *Tric-a*-overexpressing VSMCs exhibited an unexplainable abnormality in SR Ca^{2+} handling; PE-induced Ca^{2+} release was attenuated despite unchanged total Ca^{2+} content in the SR (Fig. 6*D*). In contrast, *Tric-a* knock-out VSMCs exhibit facilitated PE-induced Ca^{2+} release from the Ca^{2+}-overloaded SR (15). The alterations in PE-induced response appear to display a mirror image between *Tric-a*-overexpressing and knock-out VSMCs (supplemental Fig. S4*A*). Low Ca^{2+} contents of IP_3-sensitive stores may contribute to impaired PE-induced Ca^{2+} release in *Tric-a*-overexpressing cells because the sequential application of PE and caffeine implied poor loading in IP_3-sensitive stores (Fig. 6*H*). In this case, overexpressed TRIC-A channels may selectively gather Ca^{2+} into caffeine-sensitive stores to relatively deplete IP_3-sensitive stores in VSMCs. Because IP_3R channels are activated by both high luminal and cytoplasmic Ca^{2+} (1, 38), lowered luminal and cytoplasmic Ca^{2+} levels may synergistically inhibit IP_3R channels in *Tric-a*-overexpressing VSMCs, whereas elevated Ca^{2+} levels on both sides could facilitate IP_3Rs in *Tric-a* knock-out VSMCs. Alternatively, altered PE-induced responses could be explained by differentially modulated IP_3Rs in *Tric-a*-overexpressing and knock-out VSMCs. In addition to generating countercurrents favorable to RyR activation, the TRIC-A protein might inhibit IP_3R channels in VSMCs. These postulated inhibitory effects might be enhanced to remarkably depress PE-induced Ca^{2+} release in *Tric-a*-overexpressing VSMCs but might be removed to facilitate PE-evoked responses in *Tric-a* knock-out VSMCs. Furthermore, other molecular mechanisms can also be hypoth-

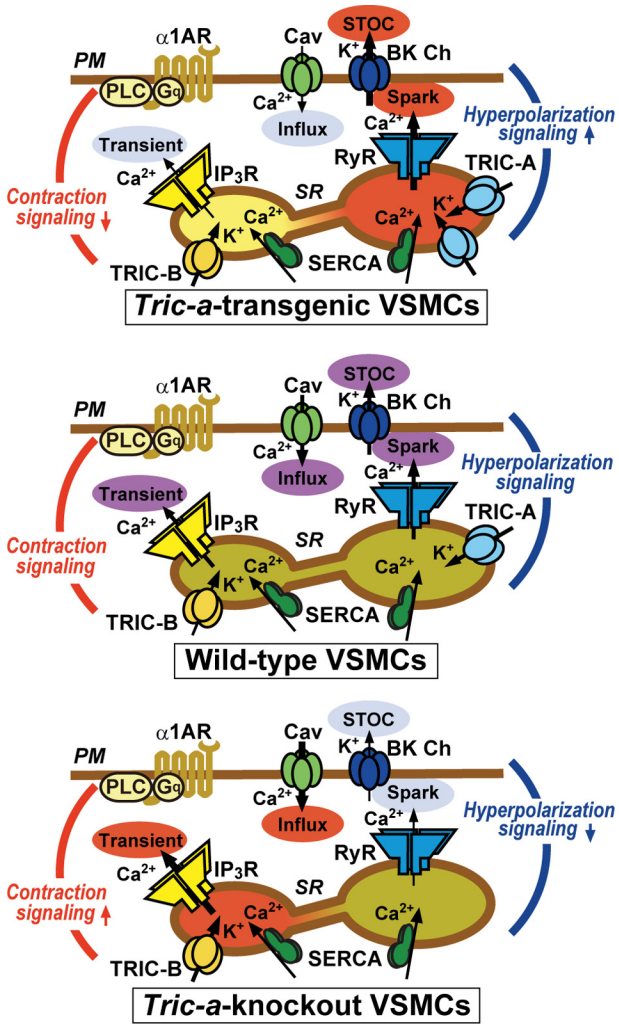

FIGURE 7. **Facilitated hyperpolarization signaling in *Tric-a*-overexpressing VSMCs.** *Tric-a* overexpression appears to activate Ca^{2+} spark generation directly, thus facilitating the hyperpolarization signaling produced by functional coupling between RyRs and BK channels (*BK Ch*) and decreasing the resting membrane potential in VSMCs. In this situation, L-type Ca^{2+} channels (*Cav*) are inactivated in the plasma membrane (*PM*), and resting $[Ca^{2+}]_i$ is decreased to develop insufficient spontaneous tonus in resistance arteries and hypotension in the transgenic mice. Upon sympathetic stimulation, the α1-adrenoreceptor (*α1AR*), trimeric GTP-binding protein G_q, and phospholipase C (*PLC*) are coordinately activated to trigger IP_3R-mediated Ca^{2+} release. In *Tric-a*-overexpressing VSMCs, IP_3R-mediated Ca^{2+} release is unexpectedly impaired. The poor agonist-induced Ca^{2+} release may be due to partial depletion of IP_3-sensitive stores or TRIC-A-mediated inhibition of IP_3Rs. In contrast, hyperpolarization signaling is impaired, and IP_3-sensitive stores are likely overloaded in *Tric-a* knock-out VSMCs (15). *SERCA*, sarco(endo)plasmic reticulum calcium ATPase.

esized for the altered PE-induced Ca^{2+} release depending upon TRIC-A contents. To further investigate the mysterious role of TRIC-A channels in IP_3-sensitive stores, physiological measurements of the mutant VSMCs under membrane-permeable "skinned" conditions together with comprehensive proteomic survey for its binding partners in Ca^{2+} stores would be required in future studies. From another point of view, it can be presumed that TRIC-A and TRIC-B channels may have distinct subtype-specific roles in SR Ca^{2+} handling. To verify this possibility, *Tric-b*-overexpressing VSMCs, producible with the use of similar transgenic technology, will provide an important model system.

In our clinical study the *TRIC-A* gene polymorphisms in the Japanese population were associated with both hypertension susceptibility and sensitivity to antihypertensive medications (15). As discussed above, TRIC-A channel density in VSMCs is an important determinant of basal blood pressure at the whole animal level. Therefore, the human hypertensive risk allele is likely associated with relatively low *Tric-a* expression in VSMCs. Hypertension represents a major health problem with an appalling annual toll, and various antihypertensive drugs have been developed. However, hypertension still remains resistant to multiple antihypertensive medications in a considerable number of patients. Although renal sympathetic denervation has recently come into use in patients with malignant hypertension, novel target proteins are still required for creating new medication strategies (40). Our transgenic mice together with the knock-out mice suggest that TRIC-A channel openers may potentially be drugs with benefits for malignant hypertension.

Acknowledgments—We thank Yuki Mizobe for technical assistance and Dr. Masamitsu Iino for valuable comments on the experimental data.

REFERENCES

1. Bezprozvanny, I., and Ehrlich, B. E. (1995) The inositol 1,4,5-trisphosphate (InsP3) receptor. *J. Membr. Biol.* **145,** 205–216
2. Meissner, G. (1994) Ryanodine receptor/Ca^{2+} release channels and their regulation by endogenous effectors. *Annu. Rev. Physiol.* **56,** 485–508
3. Berridge, M. J. (2008) Smooth muscle cell calcium activation mechanisms. *J. Physiol.* **586,** 5047–5061
4. Wellman, G. C., and Nelson, M. T. (2003) Signaling between SR and plasmalemma in smooth muscle. Sparks and the activation of Ca^{2+}-sensitive ion channels. *Cell Calcium* **34,** 211–229
5. Somlyo, A. V., Gonzalez-Serratos, H. G., Shuman, H., McClellan, G., and Somlyo, A. P. (1981) Calcium release and ionic changes in the sarcoplasmic reticulum of tetanized muscle. An electron-probe study. *J. Cell Biol.* **90,** 577–594
6. Fink, R. H., and Veigel, C. (1996) Calcium uptake and release modulated by counter-ion conductances in the sarcoplasmic reticulum of skeletal muscle. *Acta Physiol. Scand.* **156,** 387–396
7. Coronado, R., and Miller, C. (1980) Decamethonium and hexamethonium block K^+ channels of sarcoplasmic reticulum. *Nature* **288,** 495–497
8. Meissner, G. (1983) Monovalent ion and calcium ion fluxes in sarcoplasmic reticulum. *Mol. Cell. Biochem.* **55,** 65–82
9. Ide, T., Sakamoto, H., Morita, T., Taguchi, T., and Kasai, M. (1991) Purification of a Cl^--channel protein of sarcoplasmic reticulum by assaying the channel activity in the planar lipid bilayer system. *Biochem. Biophys. Res. Commun.* **176,** 38–44
10. Kamp, F., Donoso, P., and Hidalgo, C. (1998) Changes in luminal pH caused by calcium release in sarcoplasmic reticulum vesicles. *Biophys. J.* **74,** 290–296
11. Venturi, E., Sitsapesan, R., Yamazaki, D., and Takeshima, H. (2013) TRIC channels supporting efficient Ca^{2+} release from intracellular stores. *Pflugers Arch.* **465,** 187–195
12. Pitt, S. J., Park, K.-H., Nishi, M., Urashima, T., Aoki, S., Yamazaki, D., Ma, J., Takeshima, H., and Sitsapesan, R. (2010) Charade of the SR K^+-channel. Two ion-channels, TRIC-A and TRIC-B, masquerade as a single K^+-channel. *Biophys. J.* **99,** 417–426
13. Venturi, E., Matyjaszkiewicz, A., Pitt, S. J., Tsaneva-Atanasova, K., Nishi, M., Yamazaki, D., Takeshima, H., and Sitsapesan, R. (2013) TRIC-B channels display labile gating. Evidence from the TRIC-A knockout mouse model. *Pflugers Arch.*, in press
14. Yazawa, M., Ferrante, C., Feng, J., Mio, K., Ogura, T., Zhang, M., Lin, P.-H.,

Pan, Z., Komazaki, S., Kato, K., Nishi, M., Zhao, X., Weisleder, N., Sato, C., Ma, J., and Takeshima, H. (2007) TRIC channels are essential for Ca^{2+} handling in intracellular stores. *Nature* **448,** 78–82

15. Yamazaki, D., Tabara, Y., Kita, S., Hanada, H., Komazaki, S., Naitou, D., Mishima, A., Nishi, M., Yamamura, H., Yamamoto, S., Kakizawa, S., Miyachi, H., Yamamoto, S., Miyata, T., Kawano, Y., Kamide, K., Ogihara, T., Hata, A., Umemura, S., Soma, M., Takahashi, N., Imaizumi, Y., Miki, T., Iwamoto, T., and Takeshima, H. (2011) TRIC-A channels in vascular smooth muscle contribute to blood pressure maintenance. *Cell Metab.* **14,** 231–241
16. Zhao, X., Yamazaki, D., Park, K.-H., Komazaki, S., Tjondrokoesoemo, A., Nishi, M., Lin, P., Hirata, Y., Brotto, M., Takeshima, H., and Ma, J. (2010) Ca^{2+} overload and sarcoplasmic reticulum instability in tric-a null skeletal muscle. *J. Biol. Chem.* **285,** 37370–37376
17. Yamazaki, D., Komazaki, S., Nakanishi, H., Mishima, A., Nishi, M., Yazawa, M., Yamazaki, T., Taguchi, R., and Takeshima, H. (2009) Essential role of the TRIC-B channel in Ca^{2+} handling of alveolar epithelial cells and in perinatal lung maturation. *Development* **136,** 2355–2361
18. Takeshima, H., Komazaki, S., Nishi, M., Iino, M., and Kangawa, K. (2000) Junctophilins. A novel family of junctional membrane complex proteins. *Mol. Cell* **6,** 11–22
19. Ohi, Y., Yamamura, H., Nagano, N., Ohya, S., Muraki, K., Watanabe, M., and Imaizumi, Y. (2001) Local Ca^{2+} transients and distribution of BK channels and ryanodine receptors in smooth muscle cells of guinea pig vas deferens and urinary bladder. *J. Physiol.* **534,** 313–326
20. Iwamoto, T., Kita, S., Zhang, J., Blaustein, M. P., Arai, Y., Yoshida, S., Wakimoto, K., Komuro, I., and Katsuragi, T. (2004) Salt-sensitive hypertension is triggered by Ca^{2+} entry via Na^+/Ca^{2+} exchanger type-1 in vascular smooth muscle. *Nat. Med.* **10,** 1193–1199
21. Hotta, S., Morimura, K., Ohya, S., Muraki, K., Takeshima, H., and Imaizumi, Y. (2007) Ryanodine receptor type 2 deficiency changes excitation-contraction coupling and membrane potential in urinary bladder smooth muscle. *J. Physiol.* **582,** 489–506
22. Kiyoshi, H., Yamazaki, D., Ohya, S., Kitsukawa, M., Muraki, K., Saito, S. Y., Ohizumi, Y., and Imaizumi, Y. (2006) Molecular and electrophysiological characteristics of K^+ conductance sensitive to acidic pH in aortic smooth muscle cells of WKY and SHR. *Am. J. Physiol. Heart Circ. Physiol.* **291,** H2723–H2734
23. Nakano, Y., Nishihara, T., Sasayama, S., Miwa, T., Kamada, S., and Kakunaga, T. (1991) Transcriptional regulatory elements in the 5′ upstream and first intron regions of the human smooth muscle (aortic type) α-actin-encoding gene. *Gene* **99,** 285–289
24. Smith, O. A. (1974) Reflex and central mechanisms involved in the control of the heart and circulation. *Annu. Rev. Physiol.* **36,** 93–123
25. Pathak, R. K., Luskey, K. L., and Anderson, R. G. (1986) Biogenesis of the crystalloid endoplasmic reticulum in UT-1 cells. Evidence that newly formed endoplasmic reticulum emerges from the nuclear envelope. *J. Cell Biol.* **102,** 2158–2168
26. Snapp, E. L., Hegde, R. S., Francolini, M., Lombardo, F., Colombo, S., Pedrazzini, E., Borgese, N., and Lippincott-Schwartz, J. (2003) Formation of stacked ER cisternae by low affinity protein interactions. *J. Cell Biol.* **163,** 257–269
27. Tasker, P. N., Michelangeli, F., and Nixon, G. F. (1999) Expression and distribution of the type 1 and type 3 inositol 1,4,5-trisphospate receptor in developing vascular smooth muscle. *Circ. Res.* **84,** 536–542
28. Vermassen, E., Van Acker, K., Annaert, W. G., Himpens, B., Callewaert, G., Missiaen, L., De Smedt, H., and Parys, J. B. (2003) Microtubule-dependent redistribution of the type-1 inositol 1,4,5-trisphosphate receptor in A7r5 smooth muscle cells. *J. Cell Sci.* **116,** 1269–1277
29. Lesh, R. E., Nixon, G. F., Fleischer, S., Airey, J. A., Somlyo, A. P., and Somlyo, A. V. (1998) Localization of ryanodine receptors in smooth muscle. *Circ. Res.* **82,** 175–185
30. Moore, E. D., Voigt, T., Kobayashi, Y. M., Isenberg, G., Fay, F. S., Gallitelli, M. F., and Franzini-Armstrong, C. (2004) Organization of Ca^{2+} release units in excitable smooth muscle of the guinea pig urinary bladder. *Biophys. J.* **87,** 1836–1847
31. Devine, C. E., Somlyo, A. V., and Somlyo, A. P. (1972) Sarcoplasmic reticulum and excitation-contraction coupling in mammalian smooth muscles. *J. Cell Biol.* **52,** 690–718
32. Ikemoto, T., Takeshima, H., Iino, M., and Endo, M. (1998) Effect of calmodulin on Ca^{2+}-induced Ca^{2+} release of skeletal muscle from mutant mice expressing either ryanodine receptor type 1 or type 3. *Pflugers Arch.* **437,** 43–48
33. Takeshima, H., Komazaki, S., Hirose, K., Nishi, M., Noda, T., and Iino, M. (1998) Embryonic lethality and abnormal cardiac myocytes in mice lacking ryanodine receptor type 2. *EMBO J.* **17,** 3309–3316
34. Koshita, M., Hidaka, K., Ueno, H., Yamamoto, Y., and Suzuki, H. (2007) Properties of acetylcholine-induced hyperpolarization in smooth muscle cells of the mouse mesenteric artery. *J. Smooth Muscle Res.* **43,** 219–227
35. Smyth, J. T., Hwang, S. Y., Tomita, T., DeHaven, W. I., Mercer, J. C., and Putney, J. W. (2010) Activation and regulation of store-operated calcium entry. *J. Cell Mol. Med.* **14,** 2337–2349
36. Gillespie, D., Chen, H., and Fill, M. (2012) Is ryanodine receptor a calcium or magnesium channel? Roles of K^+ and Mg^{2+} during Ca^{2+} release. *Cell Calcium* **51,** 427–433
37. Iino, M. (1990) Calcium release mechanisms in smooth muscle. *Jpn. J. Pharmacol.* **54,** 345–354
38. Iino, M. (2000) Molecular basis of spatio-temporal dynamics in inositol 1,4,5-trisphosphate-mediated Ca^{2+} signalling. *Jpn. J. Pharmacol.* **82,** 15–20
39. Bolton, T. B., Prestwich, S. A., Zholos, A. V., and Gordienko, D. V. (1999) Excitation-contraction coupling in gastrointestinal and other smooth muscles. *Annu. Rev. Physiol.* **61,** 85–115
40. Laurent, S., Schlaich, M., and Esler, M. (2012) New drugs, procedures, and devices for hypertension. *Lancet* **380,** 591–600